ULTRASOUND ATTENUATION AS AN EVALUATOR OF CROSS-SECTIONAL BONE PROPERTIES

by

John R. Tedrow

Submitted to the Department of Electrical Engineering and Computer

Science in Partial Fulfillment of the Requirements for the Degrees of Bachelor

of Science in Electrical Engineering and Computer Science and Master of Engineering

in Electrical Engineering and Computer Science

at the Massachusetts Institute of Technology
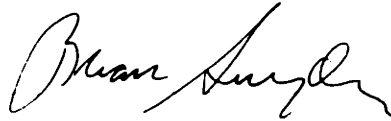
FEBRUARY 1997

©1997 John Tedrow   All Rights Reserved

Signature of Author

Department of Electrical Engineering and Computer Science
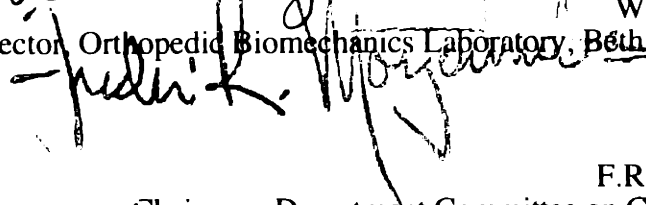February 1997

Certified by

Brian D. Snyder
Orthopedic Surgeon, Children's Hospital, Boston MA
Thesis Supervisor

Certified by

Wilson C. Hayes
Director, Orthopedic Biomechanics Laboratory, Beth Israel Hospital
Thesis Reader

Accepted by

F.R. Morgenthaler
Chairman, Department Committee on Graduate Theses

Ultrasound Attenuation as an Evaluator of
Cross-Sectional Bone Properties
by
John R. Tedrow

Submitted to the
Department of Electrical Engineering and Computer Science
February 7, 1997

In Partial Fulfillment of the Requirements for the Degree of
Bachelor of Science in Computer Science and Electrical
Enginerring and Master of Engineering in
Elerctrical Engineering and Computer Science

ABSTRACT

Fractures through bone weakened by benign tumors and metastatic cancer occur in patients of all ages and are associated with pain and loss of function depending on age, skeletal site, and associated pathology. Current radiographic guidelines for estimating fracture risk are insensitive to defect location, loading mode and are neither sensitive nor specific for predicting pathologic fracture. To develop a safe,cost effective method to predict fracture risk, I investigated whether quantitative ultrasound attenuation (QUA) could measure reductions in cross-sectional properties due to simultaed, lytic defects in trabecular and cortical bone. QUA measurements of cross-sectional properties linearly correlated with quantitative computed tomography (QCT) measures of cross-sectional area ($r^2= 0.89$) and mimimum moment of inertia ($r^2=0.79$) for trabecular bones with defects. For trabecular bone, the QUA measure of cross-sectional area also linearly correlated with compressive mechanical tests (vs. failure load, $r^2=0.77$). For cortical specimens, QUA measurements failed to correlate well with QCT or mechanical tests. However, this was shown to be due to the frequency range used for the experiment.

Thesis Supervisor: Wilson C. Hayes
Title: Director, Orthopedic Biomechanics Laboratory, Beth Israel Hospital

Acknowledgments

Over the last three years, I have had the pleasure of working in a small group which brought together a physician, a research engineer, two mechanical engineering graduate students, and an electrical engineering student to pool our resources to examine a complicated, medicine-related engineering problem. The five of us were able use each of the others' strengths to advance our own research while moving the entire group forward towards the common goal of developing non-invasive techniques of analyzing fracture risk in bones with defects.

Initially, I would like to thank Brian Snyder and John Hipp for taking a chance on me to work on this project in the first place. They have both provided the leadership and insight necessary to embark upon a project such as this one. It has been a great experience working with them.

Greg Cabe and James Hong have both provided immense assistance and support for my completing this experiment. They have both made my life a great deal easier on a number of fronts over the last few years.

Another part of the thanks must go to Professor Wilson C. Hayes for creating a laboratory like the Orthopedic Biomechanics Laboratory which fosters such groups such as ours. All the members of the lab have provided assistance at one time or another over my three years in the lab as both a UROP and graduate student.

Additionally, I would like to thank the Whitaker Foundation for providing funding for the work that is presented here. Also, Duane Morin of Walker Sonix and Hologic, Inc. provided the ultrasound equipment, answered all of my questions patiently, and never hesitated to try and help whenever he could.

Finally, the largest debt of gratitude must be paid to my mother, father, and sister. They have stuck with me over my roller-coaster career at M.I.T. and provided aid whether I realized that I needed it or not. I would not be in the position that I am in without their help.

Table of Contents

CHAPTER 1: Quantitative Ultrasound Attenuation Assessment of Cross-Sectional Properties in Trabecular Bone With Simulated Defects

1.1 Introduction

Improved guidelines are needed for preventing pathologic fractures and evaluating response to treatment in the large numbers of patients with benign and metastatic bone defects. Pathological fractures through osseous lesions in the appendicular and axial skeleton occur in patients of all ages and are often associated with intractable pain, loss of function, and other morbidities depending on the age of the patient, skeletal site and the underlying pathology. Osseous lesions that can cause pathologic fracture include malignant and benign tumors in children and metastases in cancer patients. Although malignant bone tumors in children are rare, benign skeletal defects are relatively common. Benign bone defects occur in 33-50% of asymptomatic children evaluated by random radiographs of long bones[1]. In the past ten years the Orthopaedic Oncology Service at the Massachusetts General Hospital has evaluated and treated 1716 children and young adults with benign bone defects including: non-ossifying fibroma (131), fibrous dysplasia (231), unicameral bone cyst (157), aneurysmal bone cyst (112), giant-cell tumor (426), eosinophilic granuloma (38), enchondroma (357), hemangioma (235) and chondromyxoid fibroma (29) [2]. In adults, the skeleton is the third most common site for metastatic spread of carcinoma [3]. There are over one million new cancer cases each year in the U.S.[4], and at autopsy 60-80% of cancer patients have evidence of bone metastases [5]. Approximately 30% of bone metastases subsequently fracture or produce hypercalcemia requiring treatment with radiation, bisphosphonates, glucocorticoid or calcitonin [6].

The dilemma for the orthopedic surgeon who consults in the management of these patients is multifaceted. First, one must decide if the

lesion is benign or malignant, and second, if the defect has weakened the bone sufficiently to cause pathological fracture. When pathologic fractures occur in the femur, humerus or periacetabular pelvis approximately 90% of patients require surgical intervention to relieve pain and restore function and mobility[7]. Current clinical guidelines for estimating fracture risk in adults with metastatic bone defects[8,9,10] are poorly defined and have never been proven to be sensitive or specific for predicting pathological fracture. There are also no proven guidelines for evaluating pathological fracture risk in children. Optimal treatment for bone defects is controversial[11,12,13], in part because there are no objective methods for evaluating the success of various treatment protocols. For children, possible treatments include observation, restricted weight bearing, bracing or operations to stabilize the bone and encourage healing. In contrast, radiotherapy is the principle treatment modality for adults with osteolytic metastases, although systemic treatment using cytotoxic chemotherapy, hormone manipulation, bisphosphonates and/or tumor specific radioisotopes are being investigated[14]. In addition, the methods of evaluating the state of the patient and the success of the treatment are qualitative. The prevention of pathological fracture and complications from bone metastases depends on better techniques and more objective, quantitative criteria for evaluating the tumor response to systemic and local therapy so that if a patient has failed to respond, treatment can be altered.

Quantitative Computed Tomography (QCT) is currently being used as a method of measuring cross-sectional properties of a bone, but it exposes the patient to significant ionizing radiation (as much as ten chest x-rays). In addition to the expense of obtaining CT scans, exposure to this amount of radiation is undesirable in children. Thus, the aim of this project was to investigate whether ultrasound can be used to non-invasively measure the cross-sectional structural properties of the long, weight-bearing bones of the skeleton and to predict the strength reductions associated with regularly shaped, lytic defects created in vitro.

6

Ultrasound has many practical advantages as a clinical tool for predicting strength reductions in bones with defect. It does not expose the patient to any ionizing radiation, which is beneficial not only for screening but also for multiple measurements over time to monitor a patient's response to treatment. Also, ultrasound is relatively inexpensive and portable compared to QCT, dual x-ray absorptiometry (DXA), and magnetic resonance imaging (MRI). Ultrasound is already a proven orthopaedic tool which has been used to measure bulk material properties in bones for many years and is currently used clinically for monitoring osteoporosis.

1.2 Objectives

The objective of this study was to evaluate the potential of ultrasonic attenuation for quantitatively assessing reductions in rigidity and load-bearing capacity of trabecular and cortical bone with gross, macroscopic defects. To determine this potential, the following research questions were addressed:

1. Can circular defects in regular, homogeneous specimens of trabecular and cortical bone be detected with ultrasound attenuation (QUA)?

2. What is the correlation between cross-sectional properties calculated by QUA and QCT measurements?

Answering the first question qualitatively assesses the ability of QUA to distinguish holes of different sizes in both cortical and trabecular bone and to differentiate between maximum and minimum moments of inertia. By scanning the specimens and mapping the attenuation values to a color scale, one can see a graphical representation of the specimen. It must be seen whether there is a qualitative difference between the mapping of an intact bone and that of one with a defect.

The second question provides a quantitative comparison of a variety of QUA measurements of cross-sectional properties to those measured by a "gold-

standard," QCT. Because certain cross-sectional properties, such as moment of inertia and bending rigidity provide information as to the strength of a bone, this question would provide preliminary information about the ability of QUA to evaluate the fracture risk of bones with lytic defects.

1.3 Previous Research

Broadband ultrasonic attenuation (BUA) and ultrasound velocity (UVB) have been extensively investigated as means of predicting bone density and strength. Most of these studies have been conducted with the intent of developing a clinical tool to detect and monitor osteoporosis. However, the ability of ultrasonic attenuation to predict material or structural properties of bone and the ability of any ultrasonic measure to image geometric properties of cross-sections has received much less research attention.

Ultrasound was originally investigated as a method of measuring bone properties because the speed of sound is known to be related to both the density and elastic modulus of the medium in which it is traveling, as shown in Appendix A. Using this relationship and the ultrasound velocity of propagation in bone (UVB), certain bulk material properties of the bone can be determined. Some recent studies have shown correlations between ultrasound velocity and ultimate strength of human and bovine bone as high as 0.75[15,16]. In an *in vivo* study of 16 preterm and 69 term infant cadavers, Wright found that ultrasound velocity correlated well with ultimate strength of the distal radius and ulna ($r^2 = 0.80$)[17]. Finally, UVB has been shown to correlate well with a model of bone properties involving bone mineral density (BMD) and other structural properties[18].

The slope, α_1, of the attenuation vs. frequency curve is commonly referred to as BUA. BUA has been extensively researched since it is known to be linear and its slope is material dependent in bone within a certain frequency range. BUA was first used to differentiate between osteoporotic bones and normal ones as it was found that $BUA_{normal} > BUA_{osteoporotic}$[19]. BUA and

physically-measured density correlated with $r^2 = 0.85$ in a study by McClosky and Murray of 25 *os calces* obtained from human cadavers[20]. A study of 35 *os calces* by McKelvie and Fordham produced similar correlations ($r^2 = 0.84$)[21]. In an *in vivo* study of 60 women, Langton et al. showed that women who experienced hip fractures within four weeks of a BUA measurements had significantly lower frequency-attenuation slopes than women whose hips did not fracture[22], suggesting a correlation between BUA and bone strength.

Fewer studies have investigated ultrasound attenuation. Among them, Tavakoli and Evans investigated attenuation as well as velocity of bone samples that were progressively demineralized using nitric acid[23]. They found excellent correlations between density and attenuation ($r^2 = 0.88$) as well as between density and velocity ($r^2 = 0.99$). In a separate study of trabecular bone, Evans and Tavakoli found lower correlations between attenuation and density ($r^2 = 0.56$), but found a significant observation in that in a frequency range of 0.2 MHz to 0.8 MHz, the highest correlations were at 0.6 MHz[24]. A study by Barger and a study by Langton also found that attenuation of the ultrasound wave becomes prohibitively excessive at frequency above 0.7 MHz[25] and 1.0 MHz[26], respectively. These findings suggest guidelines for choosing a frequency range for analyzing attenuation data.

1.4 Materials

Selection and Preparation of Cortical and Trabecular Specimens. Six Porcine femoral diaphyses and nine cylindrical cores from the centrums of whale vertebrae were used for cortical and trabecular specimens, respectively, in this experiment.

Porcine femurs were chosen because their diaphyses are more regularly cylindrical than those of other specimens considered. Specimens were prepared by first removing all soft tissue from the femurs. Then, a K-wire (thin metal rod) was inserted through the shaft of each specimen such that the wire was parallel to the bone axis of the mid-shaft. The alignment was

9

verified by anterior-posterior and lateral radiographs. The epiphyses of the femurs were then potted with polymethyl methacrylate (PMMA) in steel endcaps, leaving 6 cm of the mid-shaft as a gage section. During potting, the endcaps were aligned with the diaphysis at the mid-shaft by securing the K-wire in the Jacobs chucks of a lathe and positioning the endcaps with a jig attached to the lathe. The midshaft was aligned with the endcaps in order to reduce parasitic loads during mechanical testing. Once the specimens were potted, the K-wire was removed.

Trabecular bone specimens were taken from the centrums of whale vertebrae in order to secure large cores of homogeneous and transversely isotropic bone. A separate study of vertebrae from three whale species concluded that a power law relation between compressive modulus and ultimate strength applies, with statistical significance, to whale vertebral trabecular bone[27]. Furthermore, the relationships developed in that study are within the range of published equations for human trabecular bone. Finally, radiographs, QCT scans, and microMRI scans confirmed a similar architecture between whale and human trabecular bone. Based on these results, whale vertebral trabecular bone is assumed to be a valid model of human trabecular bone.

Trabecular specimens were selected from the fourth and fifth caudal vertebrae of an immature *Physeter Macrorynchus* (sperm whale) and from the sixth and eighth lumbar of a mature *Kogia Breviaceps* (pygmy sperm whale). Plane anterior-posterior and lateral radiographs were made of the intact vertebrae to roughly determine the trabecular orientation. Based on these radiographs, the superior plates of the specimens were faced and the cortical shells of the vertebrae were removed. Rectangular cores of trabecular bone were cut from the centrums with a band saw and then turned down on an EMCO Compact 5 miniature lathe to cylinders approximately 25 mm in diameter. Table 1.1 specifies the origin of each trabecular specimen. Because only nine specimen were desired, specimen DL_6 was selected at random to be

removed from the experiment.

TABLE 1.1 - Origin of Trabecular Bone Specimens

Specimen	Whale type	Lot	Vertebrae	Core #
ACa4_5	sperm	A	Caudal 4	5
ACa4_6	sperm	A	Caudal 4	6
ACa4_7	sperm	A	Caudal 4	7
ACa4_8	sperm	A	Caudal 4	8
ACa5_12	sperm	A	Caudal 5	12
ACa5_13	sperm	A	Caudal 5	13
DL6_1	pygmy sperm	D	Lumbar 6	1
DL6_2	pygmy sperm	D	Lumbar 6	2
DL8_1	pygmy sperm	D	Lumbar 8	1
DL8_2	pygmy sperm	D	Lumbar 8	2

The specimens were machined in a saline solution while frozen. When not in use, the specimens were wrapped in moist gauze and stored in sealed, evacuated plastics bags at -20° Celsius.

Selection of the Hole Site. After turning down the trabecular specimens and potting the cortical specimens, the entire lot was scanned with a GE High Speed Advantage Helical Scanner (bone algorithm, pixel size = 0.4492 mm, slice distance = 1 mm, field of view = 23 cm). The hole site for each trabecular specimen was selected to be as homogeneous as possible and free of irregularities such as vasculature. Each specimen had at least 15 mm of continuous, homogeneous bone on either side of the hole, providing a sufficiently large scan region for the ultrasound scanner. Because the cortical specimens were potted such that the midshaft cross-section of the diaphysis

11

(midway between the endcaps) was exactly parallel to the endcaps, the hole site was selected to be the mid-point of the specimen on the anterior cortex (flatter side) of the bone.

All of the specimens and their respective hole sizes are listed in Table 1.2.

TABLE 1.2 - List of Trabecular and Cortical Specimens

Specimen	Specimen Diameter D (mm)	Hole Diameter d (mm)	Ratio d/D
PA_1	22.25	4.763	19.2%
PA_2	24.81	14.288	59.5%
PA_3	22.09	7.938	35.9%
PA_4	24.85	4.763	19.2%
PA_5	25.50	7.938	31.9%
PA_6	24.00	15.875	62.2%
ACa4_5	25.14	15.875	63.1%
ACa4_6	25.03	15.875	63.4%
ACa4_7	23.53	9.000	38.2%
ACa4_8	25.35	5.105	20.1%
ACa5_12	25.82	9.000	34.9%
ACa5_13	24.7	5.105	20.7%
DL6_2	25.01	15.875	63.5%
DL8_1	25.01	5.105	20.4%
DL8_2	25.35	9.000	35.5%

1.5 Methods

The focus of this experiment is ultrasound attenuation, which measures the amount of energy lost by a sound wave as it travels between sending and receiving transducers. Attenuation is defined as $10\log_{10}(I/I_o)$, measured in decibels, where I is the measured intensity of the wave and I_0 is the initial intensity. Attenuation consists of three major components: absorption, scattering, and reflection/refraction. Absorption is the conversion of acoustic energy to heat as a wave traverses the medium. Scattering refers to the random reflection of waves due to small (compared to λ) reflectors in the medium. This component is highly dependent on frequency since frequency determines wavelength and, hence, the relative size of the wave compared to possible reflectors. The third component of attenuation is the gross reflection/refraction of energy at the boundary between two media. Reflection and refraction are functions of the impedance mismatch between two media and the angle of incidence between the sound wave and the medium's boundary.

Figure 1-1 shows the three modes of attenuation. Absorption is the dominant form of attenuation when the wavelength is much smaller than the characteristic length of the material's surface features and microstructure. Scattering begins to account for a significant amount of attenuation when the wavelength is on the order of the microstructure's size. When the wavelength is much larger than the microstructure and surface features, the specimen appears as a continuous medium to the wave, and reflection and refraction at material boundaries may dominate the energy loss, depending on the relative impedances on either side of the boundaries.

As mentioned earlier, ultrasound attenuation is sensitive to bone mass in the scan path. Therefore, ultrasound attenuation should, to some degree, measure the structural properties of a bone with a gross defect, as long as the absorption and scattering components of attenuation are much greater than the

❖ $\lambda \ll \mu$structure   **Material Prop's**
(Absorption)

❖ $\lambda \sim \mu$structure   **Microstructure**
(Scattering &
Absorption)

❖ $\lambda \gg \mu$structure   **Shape**
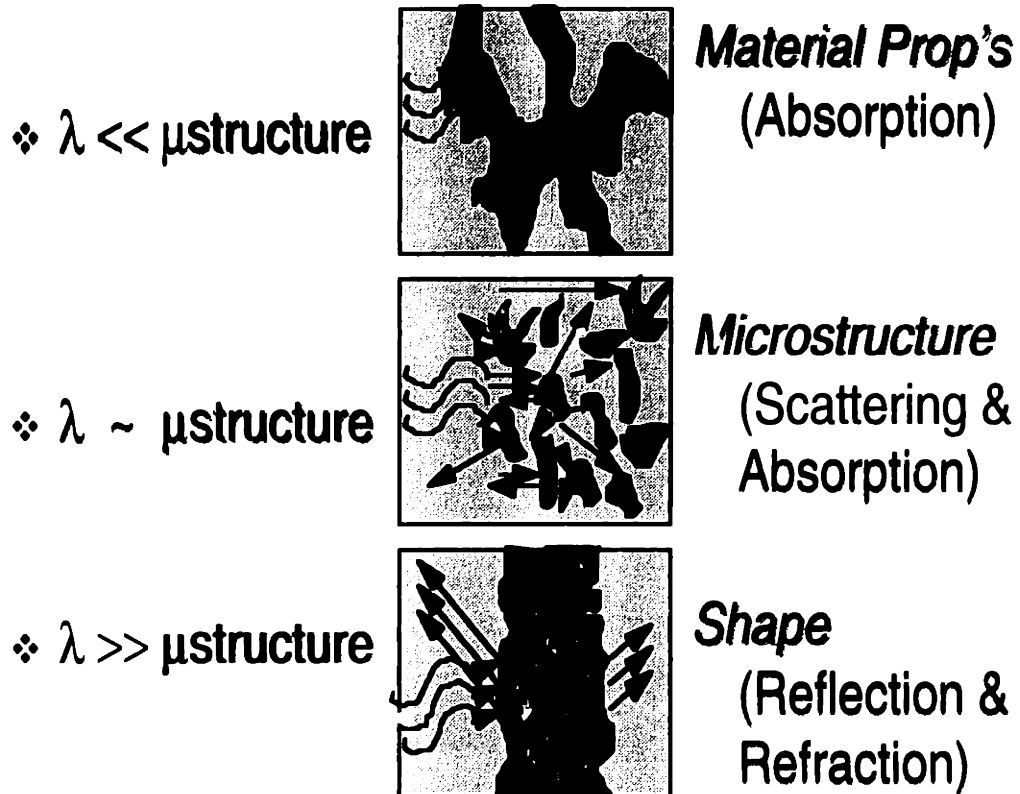(Reflection &
Refraction)

Figure 1.1 The three modes of attenuation and their dependence on wavelength
and the pore size of the medium through which the soundwaves are traveling

14

contribution from reflection and refraction. Scattering should measure the number of bone/water interfaces (e.g. trabeculae) in the wave path, and absorption should measure the material properties of the bone as well as the amount of bone in the wave path. Furthermore, using an appropriately high ultrasonic frequency should reduce the confounding effects of gross reflection and refraction. However, the frequency must also be kept low enough that attenuation does not become excessive.

Theoretically, Rayleigh scattering and absorption should be the most dominant modes of energy attenuation when the ultrasound wavelength is on the same order as the microstructure of the material[28]. Snyder et al. measured trabecular spacings on the order of 3 mm and trabecular widths on the order of 0.5 mm[29]. For bone density similar to that of the specimens in this study (0.4 g/cc to 0.6 g/cc), Ashman et al. found ultrasound velocity to be roughly 1500 m/s[30]. Studies in our laboratory have also found velocity of roughly 1650 m/s for trabecular bone[31]. The corresponding sound wavelength would be 6.6 mm for a 228 kHz wave and 2.7 mm for a 557 kHz wave. These dimensions are on the same order as the characteristic lengths of the bone microstructure. In particular, the higher the frequency, the better suited it should be suited to measuring properties of the more dense cortical bone specimens.

At the frequencies used in this experiment, the major modes of attenuation should be absorption and scattering. Thus, attenuation measured through bone would be due primarily to the amount and the material composition (rather than the shape) of attenuating media in the path of the ultrasound pulse. For example, the trabeculae in trabecular bone both scatter and absorb ultrasonic energy. When a defect is introduced, the number of trabeculae in the path of the ultrasound pulse is reduced, in turn reducing the attenuation of the ultrasound signal.

Incorporating attenuation data between 228 kHz and 577 kHz from multiple scans along a bone cross-section into quantitative variables should provide some measure of the spacial distribution of bone and, perhaps, the

material composition of the bone. This process would lead to measures of the geometric and/or structural properties of trabecular bone specimens with defects.

The ultrasound transducer apparatus used for this experiment is the same as the one described in the previous chapter. A 60 cm X 60 cm X 28 cm water tank, constructed of 0.95 cm thick Plexiglas, houses the ultrasound apparatus. This water tank is necessary to provide an interface between the transducers and the specimens. The acoustic properties of water are also close to those of soft tissue, which is an added benefit ($Z_{water} = 1.52$ X 10^6 kgm^{-2}s^{-1} and $Z_{fat} = 1.35$ X 10^6 kgm^{-2}s^{-1}). Two cradles are mounted on columns in the center of tank to position and secure the ends of a specimen. The cradles orient the long axis of the specimens parallel to the path described by the ultrasound transducers. The distance between the cradles is adjustable, and was set to 6 cm for the cortical scans and 2.5 cm for the trabecular scans. The preliminary tests confirmed that the cradles do not interfere with the scans when separated by at least 2 cm.

The transducer apparatus was modified from the Walker Sonix UBA575+ ultrasonic bone analyzer (Hologic Inc, Waltham, MA) and consists of two 1.9 cm diameter send/receive piezoelectric transducers with a characteristic frequency of 0.6 MHZ. The transducers are mounted 16.5 cm apart (which is within the length of the near field for the transducers), facing each other, on aluminum arms (see Figure 1-2). These arms are attached to orthogonal, linear motors which describe an 18 by 25 grid in 0.156 cm increments. At every point in the grid, each transducer generates a tone burst in a frequency range from 228 to 577 kHz and measures the attenuation of the burst at each frequency. The motors and transducers are controlled by a 486/33 PC which uses Orchid software (Hologic Inc., Waltham, MA) to filter, process, and store the attenuation data.

A Norland Stratec XCT 960A peripheral QCT scanner was used for quantitative computed tomography scans of the specimens. This technology is

16

Figure 1-2 The ultrasound transducer apparatus, water tank, and jig for holding specimens

common and well-developed, and is, therefore, not described in further detail here.

QUA and QCT Scans. Before holes were introduced, the trabecular and cortical specimens were scanned in the peripheral QCT scanner, using a pixel size of 0.295 mm and a slice distance of 3 mm. The scanning procedure resulted in inaccurate measurements of specimen density, and hence modulus. However, the inaccuracy was minimal, and did not affect the final results.

The specimens were also scanned with the modified ultrasound apparatus. The cortical and trabecular specimens were each degassed in 0.9 M saline for 2 and 4 hours respectively. The ultrasound tank was filled with distilled water and allowed to settle, and then a baseline ultrasound scan was taken of the water-filled tank with no specimens. After the baseline scan, specimens were transferred under water one at a time to the ultrasound tank and secured in the cradle using a marker to accurately position the hole. Each specimen was first scanned with the long axis of the intended hole oriented perpendicular to the oncoming ultrasound wave as shown in Figure 1-3. Each specimen was then scanned at a series of three 45-degree rotations about its long axis ($0°$, $45°$, $90°$, $135°$). The 0-degree orientation corresponds to the QCT orientation for Ixx (Imin after holes were drilled), and the 90-degree orientation corresponds to the QCT orientation for Iyy (Imax after the holes were drilled).

Transverse, circular holes were introduced into each specimen at the pre-selected hole site using titanium-nitride-coated and pilot-point drill bits at 3000 RPM. The drill bits were stepped in size in order to reduce micro-fractures introduced by the bits grabbing specimen edges during machining. Because lytic defects in long bones often span the entire width of the trabecular region but usually only penetrate one cortex of the bone, holes were drilled through the entire cross-section of the trabecular specimens and through only one cortex of the cortical specimens. The cortical specimens were randomly placed in 3 groups of 2, and the trabecular specimens were
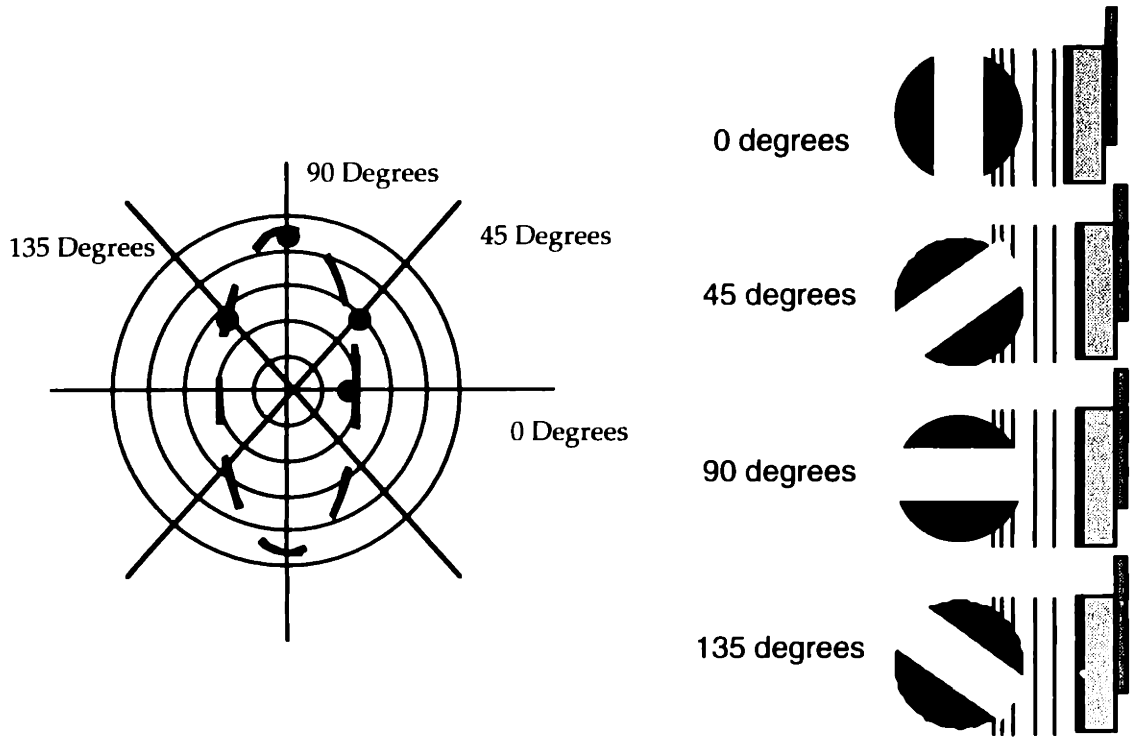
18

Figure 1-3 The cartoon on the left represents a polar plot of moment of inertia plotted against angle of rotation with respect to the transducers (on right)

19

randomly placed in 3 groups of 3. Each group was then randomly assigned a target defect diameter - either 20%, 35%, or 60% of the nominal cross-sectional area of the specimen.

After the holes were introduced, the specimens were scanned in the same manner as before with the peripheral QCT scanner and the ultrasound apparatus. In order to establish the precision of the ultrasound data, the cortical specimens with defects were each scanned twice with the ultrasound apparatus.

1.6 Techniques for analyzing image data

QCT Data Analysis. QCT acquires data by rotating an x-ray source and detector around the specimen. Measurements of x-ray attenuation are taken at each source-detector angle. The information is stored as entries in a matrix of attenuation measurements called CT numbers (in Hounsfield units), each of which corresponds to the density of a volume element of bone at the given location in the cross-section.

The GE Hi-light Helical clinical scanner produces a 512 x 512 matrix of CT numbers. During the scan, a 6-chamber solid calcium hydroxyapatite phantom is imaged with the specimen. A linear relationship is then derived correlating the CT numbers for the chambers with the known chamber densities. This relationship is then used to map CT numbers of the bone to bone density for each voxel (volume element). Young's modulus is then calculated for each voxel using an empirical relation. The Norland Stratec XCT 960A peripheral QCT scanner also produces a 512 x 512 matrix of CT numbers. They are mapped to density using a calibration measurement of a density phantom taken before scanning of the specimens.

Various geometric, material, and structural properties of a cross-section are calculated using modified composite beam theory, implemented as an AVS (Advanced Visualization Systems, Waltham, MA) module. Each three-

dimensional voxel in a cross-section is collapsed through its thickness and analyzed as an equivalent two-dimensional pixel.

The average density (modulus) of the cross-section is calculated by summing the density (modulus) of all the pixels above a specified density threshold and dividing by the total number of pixels:

$$\rho = \frac{\Sigma_1^n \rho_i}{n} \qquad [1]$$

$$E = \frac{\Sigma_1^n E_i}{n} \qquad [2]$$

where

ρ_i = density of the ith pixel

E_i = Young's modulus of the ith pixel

Cross-sectional area is calculated by simply summing the number of pixels of CT number greater than a specified density threshold multiplied by the individual pixel area. Similarly, axial rigidity is calculated by weighting the area with the modulus of each pixel:

$$A = \Sigma_1^n A_i \qquad [3]$$

$$AE = \sum_{1}^{n} A_i E_i \qquad [4]$$

where

A_i = cross-sectional area of ith pixel

In a like manner, geometric and modulus-weighted neutral axes are calculated, as are other properties, such as moment of inertia and bending rigidity:

$$\bar{x}_{geo} = \frac{\sum_{1}^{n} x_i A_i}{\sum_{1}^{n} A_i} \qquad [5]$$

$$\bar{x}_{struct} = \frac{\sum_{1}^{n} x_i E_i A_i}{\sum_{1}^{n} E_i A_i} \qquad [6]$$

where

x_i = x coordinate of centroid of ith pixel

and

$$I_{yy} = \sum_{1}^{n} (x_i - \bar{x})^2 A_i \qquad [7]$$

22

$$EI_{yy} = \sum_{1}^{n} (x_i - \bar{x})^2 E_i A_i \qquad [8]$$

where

x_i = distance from neutral axis to centroid of ith pixel

I_{yy} = moment of inertia about y-axis

Quantitative Ultrasound Attenuation Data Analysis. QUA in this experiment acquires data by measuring ultrasound energy attenuation (dB) as transducers are effectively rotated 135 degrees (in increments of 45 degrees) around a specimen. The scanner generates an 18 by 25 matrix of attenuation values at each orientation of the transducers with respect to the specimen. One matrix is generated for each of 27 frequencies, ranging from 228 kHz to 577 kHz.

For each specimen, a representative 25-point column from the matrix of attenuation data is chosen for analysis (see Figure 1-4). A cubic spline is fit to a plot of $g(x_i)$ versus scan position and cut off at a baseline which is established by measuring the signal attenuation in the water-filled tank without a specimen. The cubic spline describes a "profile" of attenuation vs. scan position for the specimen. The ultrasound attenuation, $g(x_i)$, at each scan point, x_i, across the bone cross-section is thought to depend heavily on the amount of bone in that scan. Therefore, the attenuation profile should provide some representation of the spacial distribution of bone mass.

The area between the curve and the baseline is calculated using a trapezoidal numerical integration scheme:

$$S1 = \int g(x) dx \qquad [9]$$

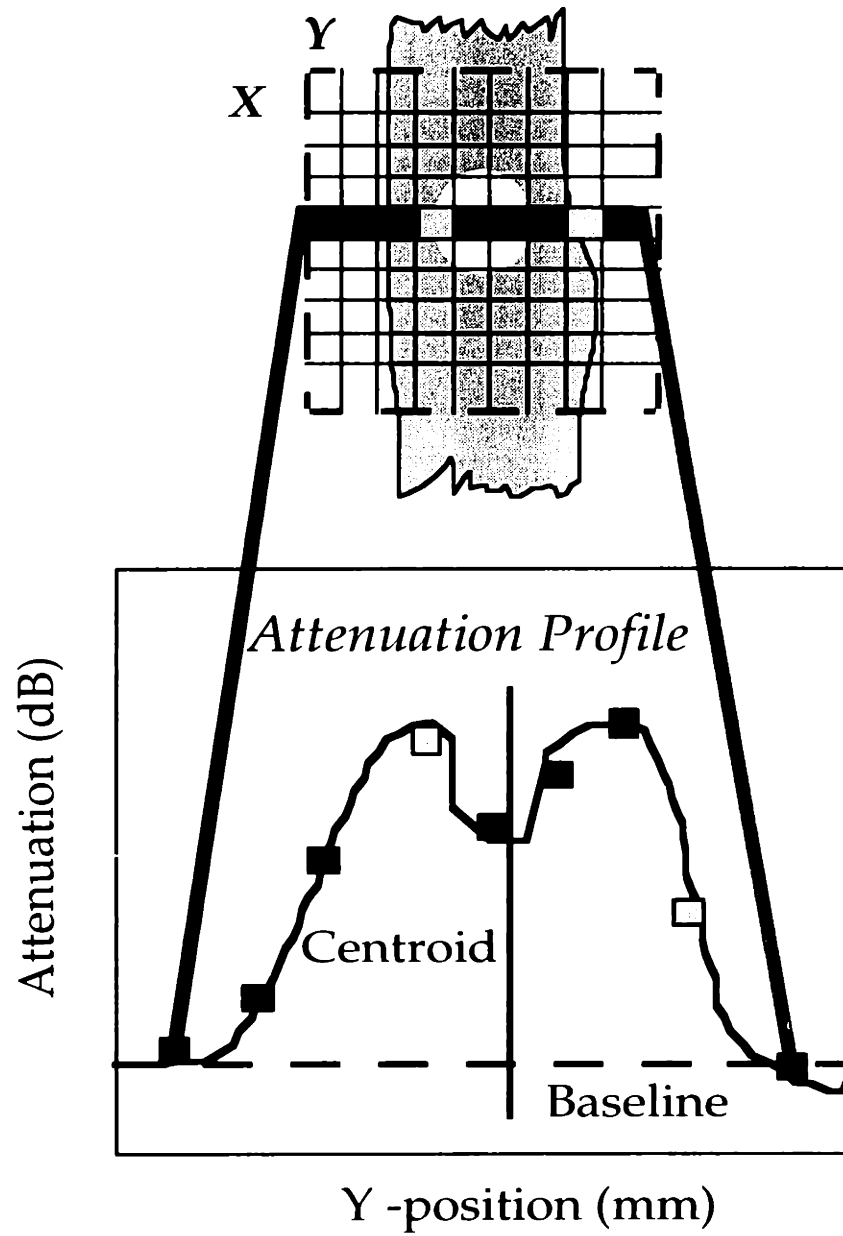A centroid, x', for the curve is also found, and the second moment of the curve about the centroid is calculated:

Figure 1-4 This cartoon represents the generation of an
attenuation curve. In a real scan, there are 25 points plotted

24

$$S2 = \int g(x_i)x_i^2 dx - Sx'$$ [10]

S1 should be a scaler quantity which corresponds to cross-sectional area or axial rigidity, and S2 should be a vector quantity (dependent on scan orientation) which should correspond to either moment of inertia or bending rigidity. Using values of S2 from multiple orientations of the specimens with respect to the sound wave source, the principle values of S2 can be found from the associated eigensolutions.

1.7 Results and analysis

Research Question 1

"Can circular defects in regular, homogeneous specimens of trabecular and cortical bone be detected with ultrasound attenuation (QUA)?"

Figure 1-5 shows color-scaled maps (all using the same scale) of attenuation for an intact trabecular specimen, three trabecular specimens with different size transverse holes, and a cortical specimen with a unicortical hole. The scans were performed with the long axis of the hole parallel to the wave path. There is an obvious, visual progression from one hole size to the next. Figure 1-5 shows the attenuation profile at the "center" cross-section of the hole from each of these species. Once again, there is an obvious progression in hole size and a difference between the cortical and trabecular specimen with the same hole size. However, the 20% defects (5.1 mm) were at the low end of the resolution of the 19 mm diameter transducers and were therefore less visible.

The attenuation profiles also indicate, qualitatively, the changes in cross-sectional area for different orientations of the hole with respect to the bending axis. Figure 1-6 shows the attenuation profiles for a 60% hole in trabecular bone at angles of the hole with respect to the transducers of 0, 45, 90, and 135

25

degrees. The scan at 0 degrees corresponds to the orientation for the minimum bending moment of inertia, and the scan at 90 degrees corresponds to the orientation foi the maximum bending moment of inertia.
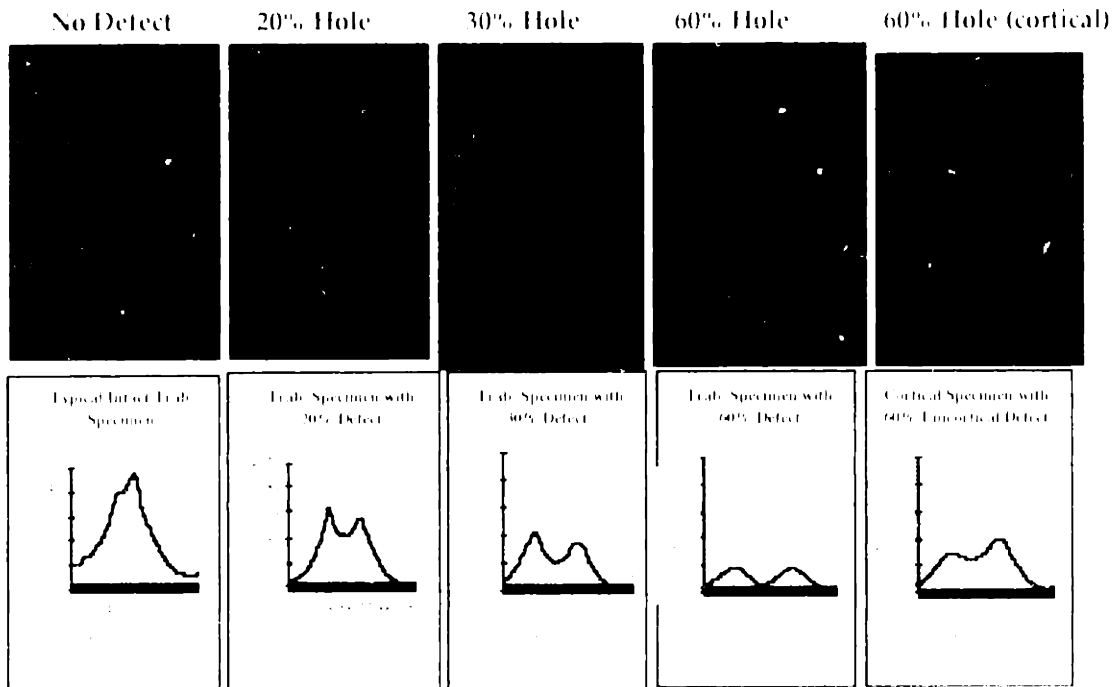
No Defect	20% Hole	30% Hole	60% Hole	60% Hole (cortical)

Figure 1-5 The upper row are maps of the 18 X 25 array of attenuation values in an ultrasound scan (the red is high attenation and the blue is low on a ROYGBIV color scale) The lower row of graphs represent an attenuation curve through the center of the hole region of each specimen
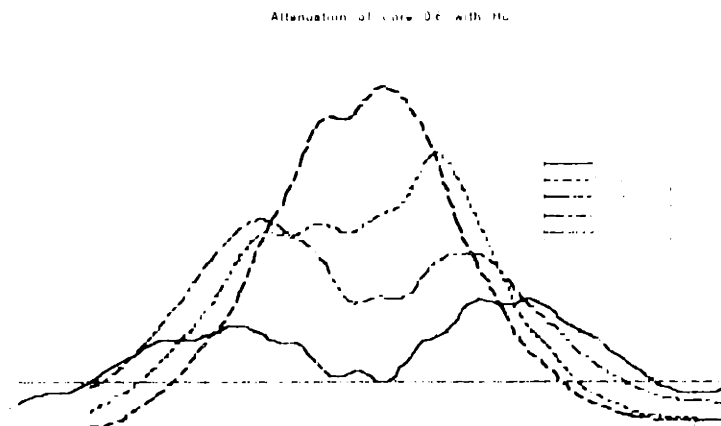

Figure 1-6 Attenuation curves for a trabecular core with a 0 6 d D defect rotated at 0 45 90 and 135 degrees

Research Question 2

"What is the linear correlation between cross-sectional properties calculated by QUA and QCT measurements?"

This research question was answered by investigating the correlations between QUA measurements and QCT measurements based on a 3 mm thick slice at the hole site. As discussed previously, QUA S1 should be a scaler quantity which corresponds to cross-sectional area (A). So, the average S1 for all scan angles was correlated to A as measured by QCT. QUA S2 should be a vector quantity which corresponds to moment of inertia. So, the major and minor axes of the ellipse fit to the S2 data were correlate to QCT measures of Imax (EImax) and Imin (EImin), respectively.

A probable clinical ultrasound technique would be to compare ultrasound measurements of a pathologic limb to those of the healthy, contralateral limb. Therefore, correlations between QUA and QCT measurements were studied as reductions in bone properties due to the introduction of a hole. The reductions were expressed as a measurement of a specimen with a defect normalized to that of a specimen without a defect. In order to assess the ability of ultrasound to predict the absolute measure of a property, QUA and QCT measurements were also compared by plotting measurements of specimens before the defects were introduced on the same graph as measurements after the defects were introduced. The correlations were investigated for trabecular and cortical specimens separately.

Geometric Properties - Trabecular Specimens.

The linear regressions for absolute measurements of the cross-sectional area and minimum moment of inertia for the trabecular specimens before and after hole introduction were very good. The correlation between A and S1 was very strong ($r^2 = 0.89$, $p < 0.001$, see Figure 1-7). Additionally, S1 showed no significant relation to orientation. It correlated equally well with QCT area at each scan angle, as would be expected for a scaler quantity like area. The

28

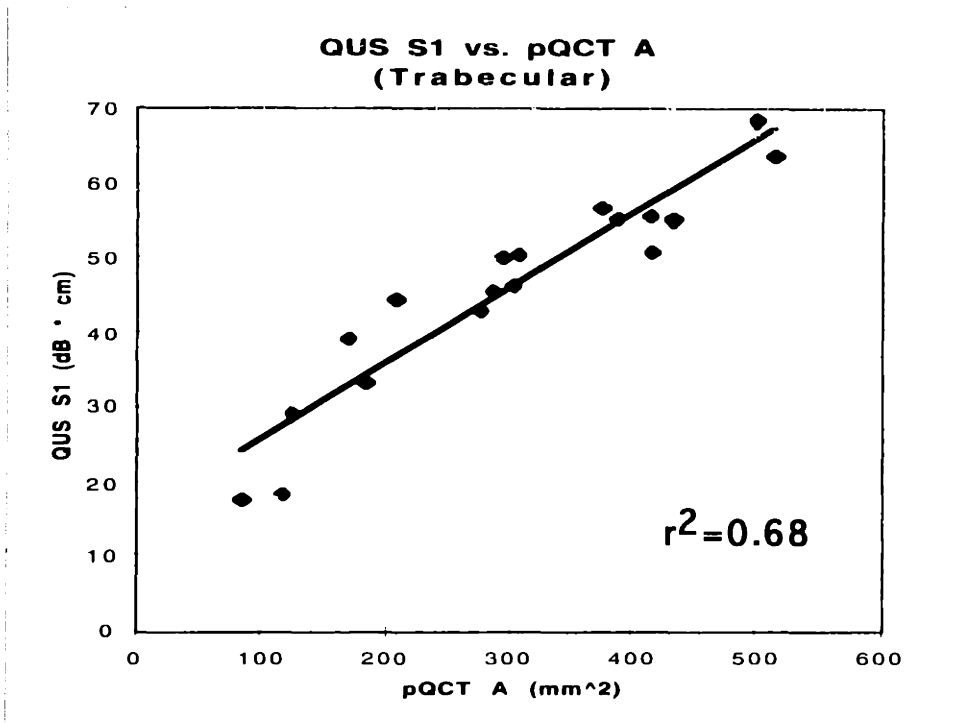correlation between Imin and S2min was also strong ($r^2 = 0.80$, p < 0.001, see

QUS S1 vs. pQCT A
(Trabecular)

$r^2 = 0.68$

Figure 1-7 Linear regression of QUS measured S1 vs. pQCT measured

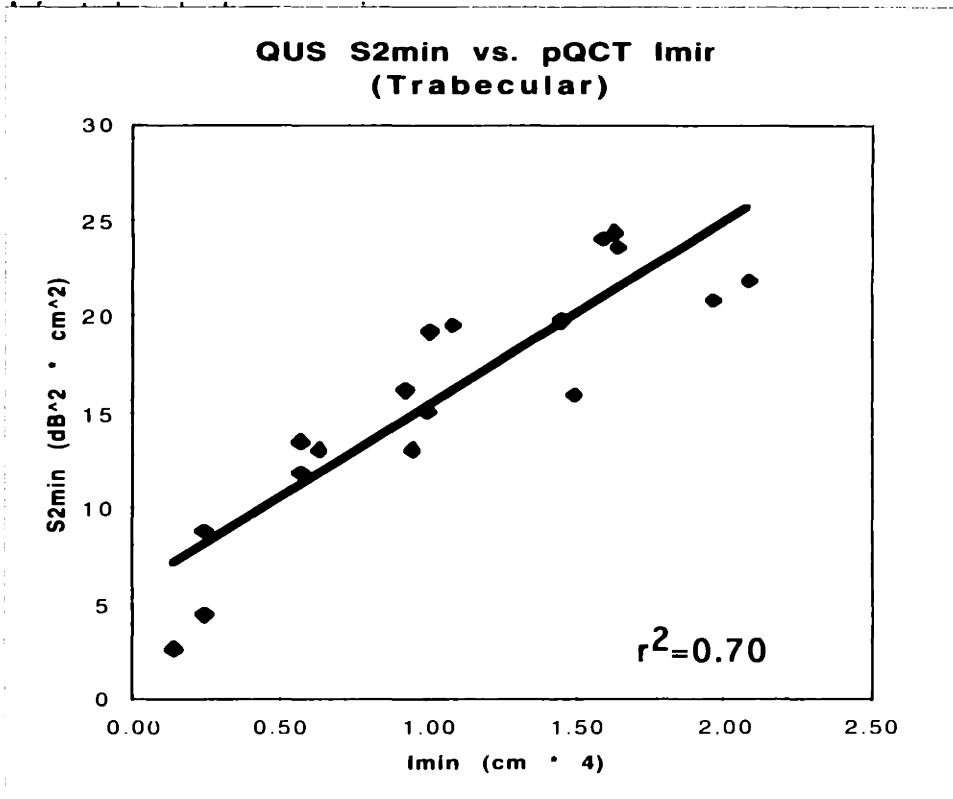**QUS S2min vs. pQCT Imir**
(Trabecular)

$r^2 = 0.70$

Figure 1-8 Linear regression of QUS S2min vs. PQCT Imin for trabecular bone specimens

30

Figure 1-8), although there was no correlation between Imax and S2max (r^2 = 0.06, p< 0.5).

The regressions between normalized (specimen with defect:: intact specimen) QUA measurements (S1, S2min, S2max) and normalized QCT measurements (A, Imin, Imax) for the trabecular specimens should give an indication as to how ultrasound measures the reduction in cross-sectional properties. The correlation (see Figures 1-9 and 1-10) between Imin and S2min ratios and that for S1 and A ratios were each very strong (r^2 = 0.70, p<.001 and r^2 = 0.68, p<.001 respectively). However, the S2max ratio to Imax ratio correlation was extremely weak (r^2 = 0.02, p<.001).

Although QUA's S2 inaccurately measured the angular dependence of moment of inertia, it did agree with QCT on the orientation for minimum moment of inertia in 12 out of 15 scans of bones with holes and 10 out of 15 scans of bones without holes. The ability to measure the minimum load capacity and the corresponding load orientation in a bone with a defect is of greater clinical importance than quantifying maximum load capacity.

Geometric Properties - Cortical Specimens. The same QUA and QCT measures discussed above were calculated for the cortical specimens as an independent specimen lot, and the linear regressions are shown in Figures 1-11 and 1-12. The correlations were not high for all of the data. The correlation for S2min vs. Imin was r^2 = 0.76 (p<0.001), S2max vs. Imax was r^2 = 0.57(p<.01), and S1 vs. A was r^2 = 0.62 (p<1). The regressions for the ultrasound calculations and QCT calculations for the S2min to Imin ratios (r^2=0.43, p<0.001) are shown in Figure 1-13 . There was virtually no linear correlation between the cross-sectional area ratios (r2=0.10, p<0.001).

1.8 Discussion

There are four probable reasons for the low correlation between S2max and Imax in virtually every case. First, the variation in Imax was much less

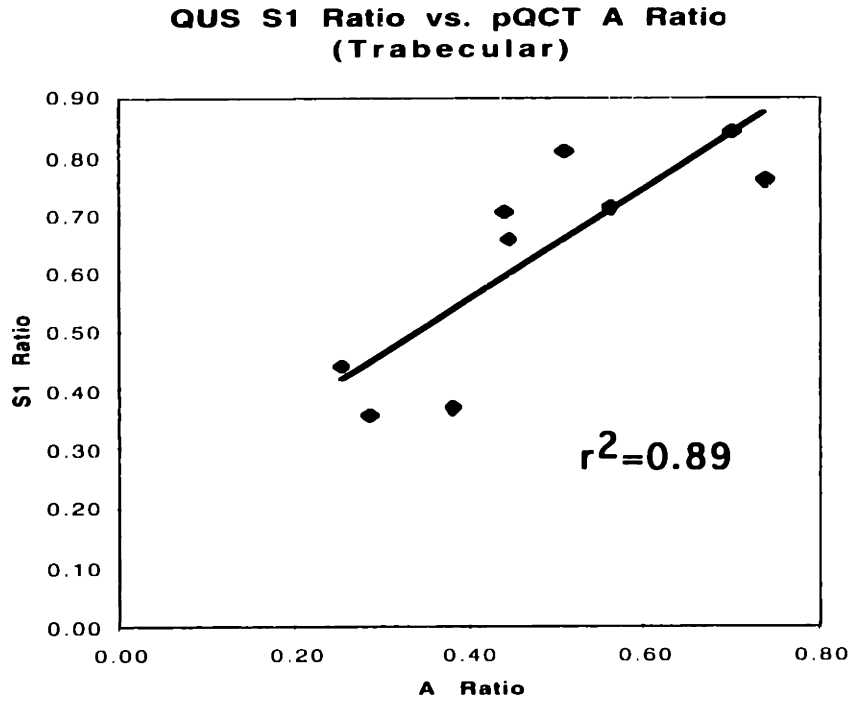**QUS S1 Ratio vs. pQCT A Ratio
(Trabecular)**

$r^2 = 0.89$

Figure 1-9 Linear regression of QUS S1 ratio vs. PQCT measured A
ratios for trabecular bone specimens

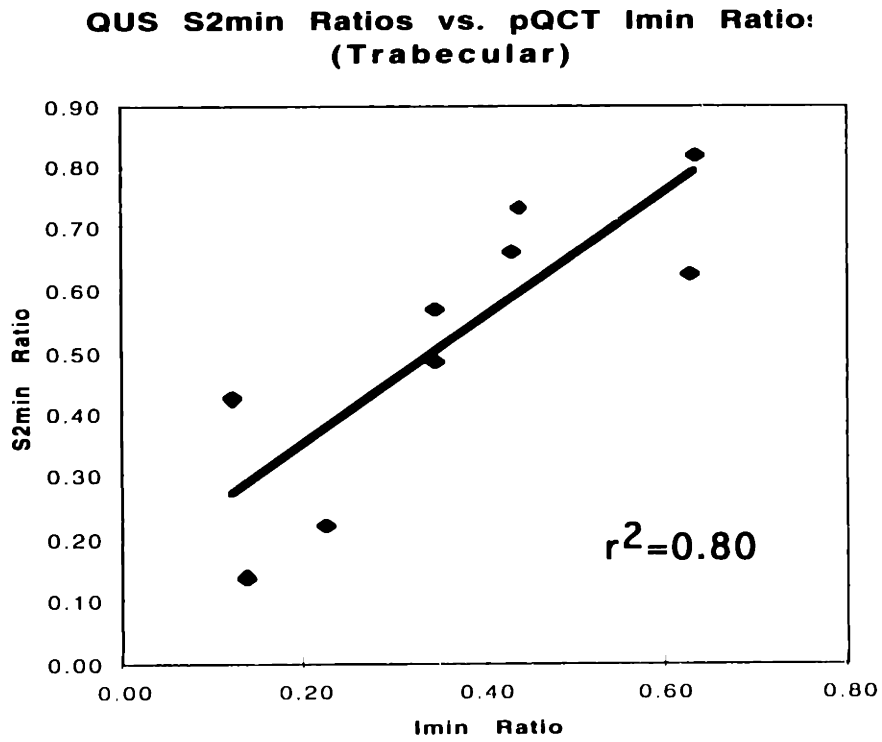**QUS S2min Ratios vs. pQCT Imin Ratio:
(Trabecular)**

$r^2 = 0.80$

Figure 1-10 Linear regression of QUS S2min Ratios vs. PQCT Imin
Ratios for trabecular bone specimens

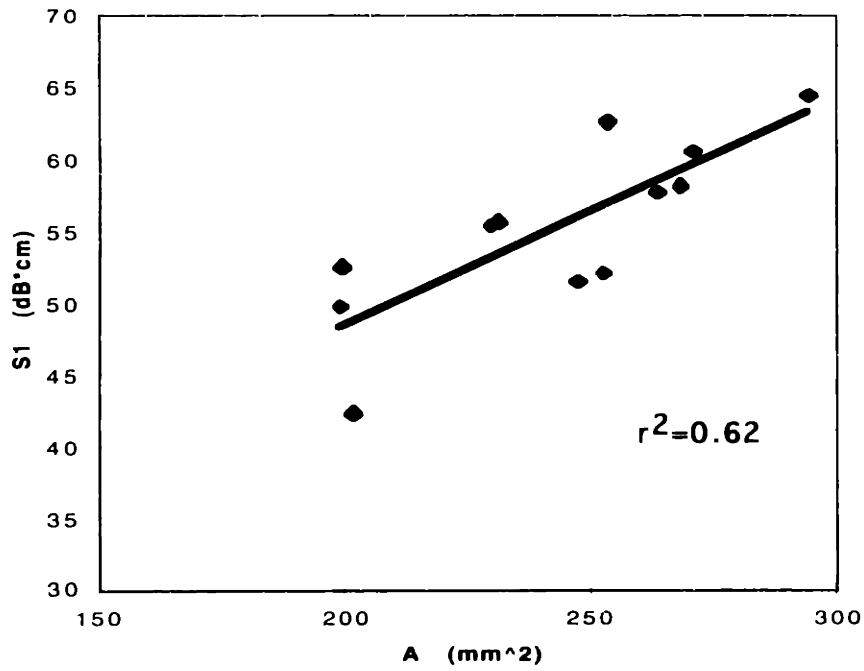**QUS S1 vs. pQCT A (Cortical**

Figure 1-11 Linear regression of QUS S1 vs. pQCT a for cortical bone
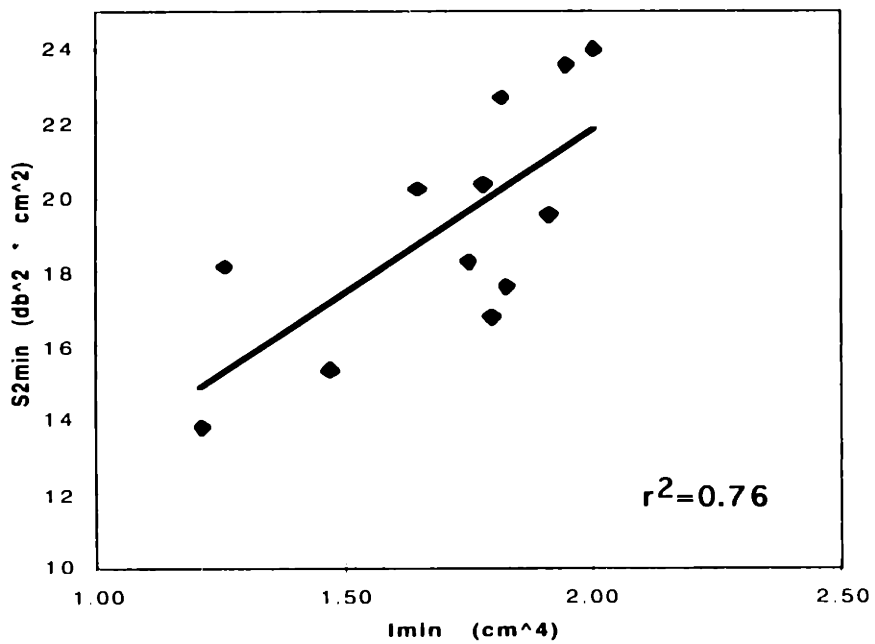s

**QUA S2min vs. pQCT Imir
(Cortical)**

Figure 1-12 Linear regression for QUA S2min vs. pQCT Imin for
cortical bone specimens

33

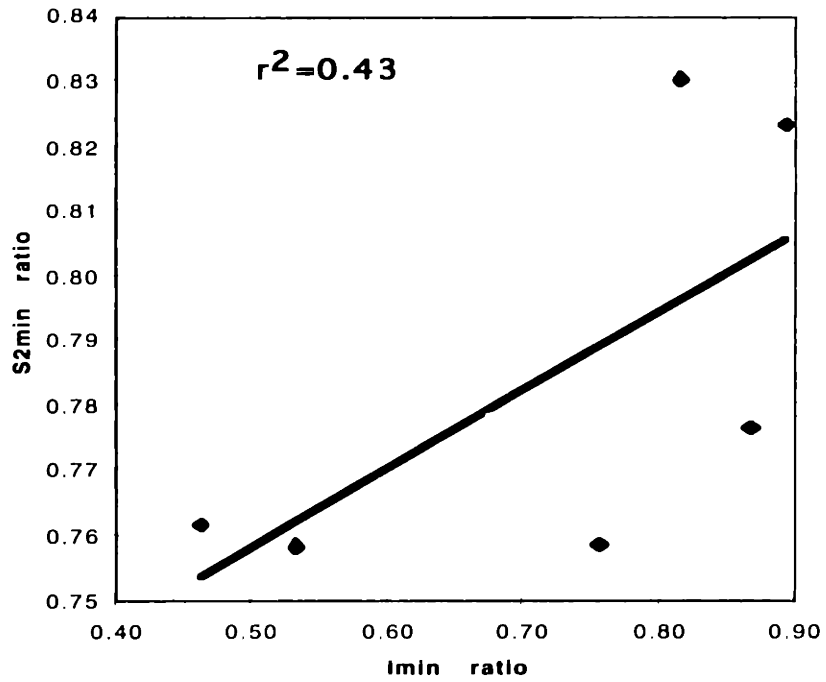**QUS S2min ratios vs. pQCT Imin ratio
(Cortical)**

$r^2 = 0.43$

Figure 1-13 Linear regression for QUA S2min ratios vs. PQCT Imin ratios for cortical bone specimens

than the variation in Imin, therefore the regression for Imax may have been weak because of the small range that it covered. Another reason may be that there was sufficient gross reflection and refraction to distort the signal. Reflection/refraction distortions would be maximized and spacial distribution of bone mass would be minimized at the orientation in which S2max was measured. The reverse would be true for the S2min orientation. Additionally, in 24 out of 30 specimen measurements, ultrasound measured higher values for S2 at 45 and 135 degrees than at 90 degrees, which is inconsistent with the angular dependence of moment of inertia and indicates that scans at these angles may adversely bias the ellipse fits. Finally, the correlations may be weak because the ultrasound pulse is 19 mm in diameter - 75% the diameter of the entire specimen and 370% the diameter of the smallest hole. Smaller or focused transducers isolate smaller regions of the specimen at each data point and may, therefore, produce more accurate measurements. This volume-averaging problem worsens the correlations for all of the cases.

The cortical specimens showed weaker correlations than trabecular specimens in every measurement. However, this may be due in part to the smaller number of cortical specimens and to the fact that the cortical specimens spanned a much smaller range of areas and moments of inertia than did the trabecular specimens. Additionally, the cortical specimens would be more susceptible to the reflection problems outlined earlier, due to the small pore size associated with the haversian canals.

CHAPTER 2: Quantitave Ultrasound Assessment of Fracture Risk in Bone With Simulated Lytic Defects

2.1 Overview

The overall objective of the grant funding this study is to develop practical, cost-effective, and non-invasive methods for predicting fracture risk in children and adults with osteolytic defects and pathological skeletal deformities. It is hoped that analytic techniques can be developed which will facilitate patient management and resource utilization by providing guidelines for selecting among the various treatment options based on predicted fracture risk. These same techniques will also provide an objective method for evaluating the patient's response to treatment.

Quantitative ultrasound has shown the potential to measure cross-sectional properties in bone, but this result must be further examined to show whether or not these measures have physical significance in terms of fracture risk. If ultrasound can assess strength reduction associated with lytic defects, it could provide a valuable tool for clinical use. Due to its low cost and lack of ionizing radiation, ultrasound would be ideal for diagnosis and follow-up for patients with the sorts of conditions outlined in Chapter 1.

2.2 Research Question

1.   What is the correlation between QUA and QCT measured cross-sectional properties of trabecular and cortical bone and elastic rigidity/failure load of trabecular specimens in compression and cortical specimens in four-point bending?

Even though QUA can measure some cross-sectional properties, it is necessary to see if these measurements have physical significance.   If the QUA measurements do relate to the real mechanical data, that would provide

the strongest proof that QUA has the potential to be a useful clinical tool. The QCT data also needs to be compared with mechanical data to make sure that it is the gold standard that it was assumed to be in the previous chapter.

2.3 Materials

The specimens described in section 1.4 were also used for this part of the study. The mechanical tests were performed on the specimens after the defects (see Table 1.2) were created.

2.4 Methods

Mechanical Testing of Femurs. In order to answer the research question, cortical specimens were tested in four-point bending after the holes were drilled. Four-point bending was the most appropriate mechanical test based on the geometry of the specimens.

The cortical specimens were tested destructively in 4-point bending using an Instron 8500 test frame and an Instron 8511 controller and signal conditioner. The displacement of the center cross-section was measured using the Mac Reflex optical system (Qualysis, Sweden). This system consists of cameras which produce a pulse of infrared light. These video cameras record the position of infrared light reflected off a marker glued in line with center of the hole along the neutral axis of the bone specimen. The load frame was controlled by a single ramp to failure at a strain rate of .05/s. The load and cross-head displacement were also measured with a force transducer and an LVDT.

Mechanical Testing of Trabecular Cores. Because of the short length of the specimens, compared to their diameter, compression was the natural mode of mechanical testing for the trabecular specimens. The specimens were destructively tested by uniaxial compression. Using the same Instron hydraulic load frame under displacement control, each specimen was compressed at a

strain rate of .01/s. Failure load and axial rigidity were measured.

2.5 Results

Research Question

"What is the correlation between QUA and QCT measured cross-sectional properties of trabecular and cortical bone and elastic rigidity/failure load of trabecular specimens in compression and cortical specimens in four-point bending?"

The four-point bending data correlated very well with the pQCT results. The failure load correlated strongly with moment of inertia (r^2=0.84, p<0.01). However, the ultrasound S2 values failed to correlate with these data. The correlation between S2min and the yield load was r^2=0.18 (p<0.5). The regression is shown in Figure 2-1.

Failure load of the trabecular specimens was measured from the compressive tests. This measurement should depend on cross-sectional area. This dependence was borne out for failure load by the strong correlations with QCT measured cross-sectional area (r^2=0.81 for QCT (p<0.001)). Ultrasound S1 also linearly correlated (see Figure 2-2) very strongly with failure load (r^2=0.77, p<0.001), directly demonstrating that the ultrasound calculated value has physical significance.

2.6 Discussion

Cortical Tests

There are several possible reasons for why the QUA measurements failed to linearly correlate with the mechanical tests. The first is that, due to the frequency range analyzed, the properties calculated for the cortical specimens by QUA were not well correlated with the pQCT results, and thus were not a good indicator of the mechanical properties of the bones either. Additionally, the ultrasound measurements were more geometric in nature,

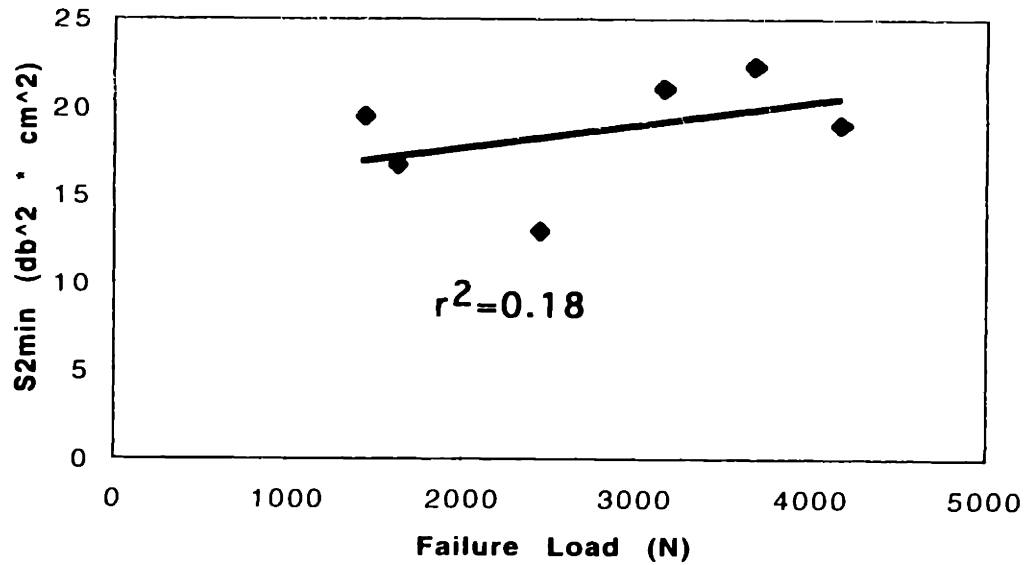**Bending Failure Load vs. S2mi**

Figure 2-1 Linear correlation of bending load vs. QUA calculated S2min for cortical specimens
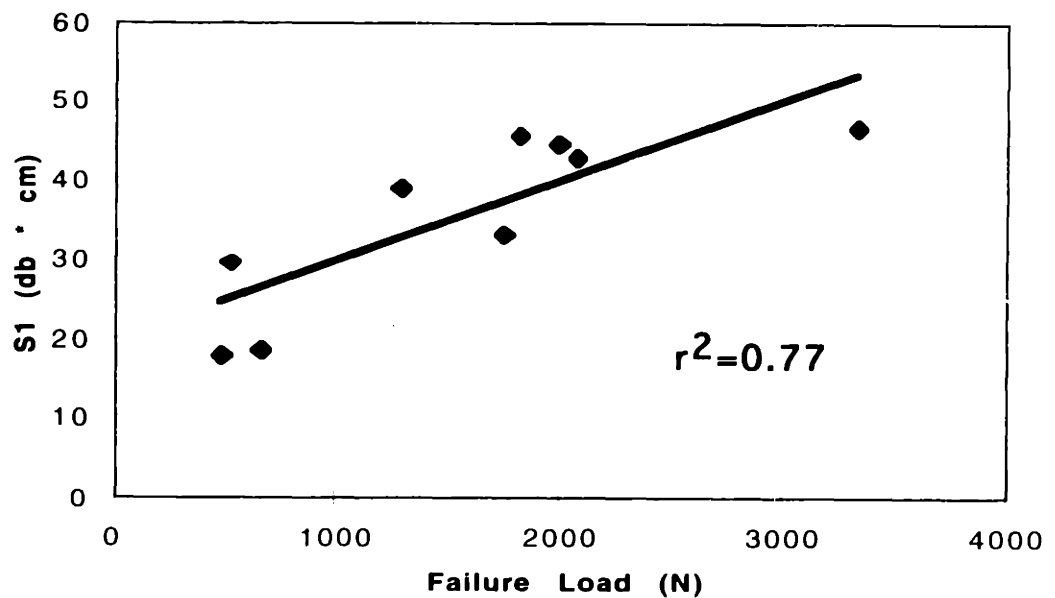
Compressive Failure Load vs. S

Figure 2-2 Linear correlation of compressive failure load vs. QUA calculated S1

and did not necessarily reflect the structural properties of the bones. Most likely, it is a combination of these two effects that caused there to be no correlation between the mechanical tests and the QUA calculations.

Trabecular Tests

The good correlations between QUA S1 and failure load means that the ultrasound measurements have some physical significance.

These two results imply that it is possible to non-invasively determine the cross-sectional properties of bones. However, more development must occur in the cortical case to determine structural properties from ultrasound attenuation. This development should include different, higher frequency ranges and trying to glean modulus information from the velocity of the sound waves in bone to try and get closer to the structural properties.

CHAPTER 3:The Effect of Reflection on Attenuation

3.1 Overview

The results from the previous experiments require further investigation. The results are obviously much better for the trabecular specimens than for the cortical specimens. In fact, there was basically no correlation between the mechanical testing data and the calculated ultrasound parameters. There are several possible explanations for this result. Due to the fact that the QCT measurements did correlate with the mechanical test data, the flaw most likely lies within the ultrasound method.

There was a major assumption made for the attenuation curve method to work: that the major modes of attenuation were absorption and scattering rather than gross reflection. What modes of attenuation dominate are primarily determined by the frequency of the ultrasound wave. If the wavelength of the sound wave is very large compared to the matrix of the specimen, the wave will behave as if it is contacting a contiguous medium rather than a porous structure. In this scenario, there will be a large amount of reflection. This type of attenuation will not provide any information about the structure of the specimen being scanned. Moreover, if the reflection is not complete, but is only a major component of the total attenuation, this sort of reflection will skew the resultant attenuation curves.

In order to gauge the effect of reflection, another experiment had to be performed. Ideally, one could set up a specimen such that one could scan it several times with only the reflection component of the attenuation changing. To this end, thin wafers of bone with different porosities were cut and held in a position perpendicular to the path of the ultrasound beam. These specimens were scanned, and then rotated about one end as to cause the sound waves to be reflected in different directions. In this case, the amount of attenuation would be dependent on angle of rotation if reflection is a major component,

and otherwise, the attenuation would be insensitive to angle. Furthermore, it should be possible to measure the reflective peak in each transducer in the perpendicular case and compare it to the peak of the transmitted signal.

3.2 Research Question

1.   Does gross surface reflection alter the overall attenuation measured through a bone specimen?

3.3 Materials

Six parallelepipeds of bone were cut from two vertebrae from a bow head whale (*baelena mystecetus*). These specimens were cut to be 70 mm X 70 mm X 5 mm. The two particular vertebrae were chosen as to give a large range of bone densities. The first had an ash density of approximately 0.5 g/cc and the second had an ash density of 1.3 g/cc. Due to the large transducer size, one needs broad specimens so that the attenuation data is not influenced by effects at the edges of the specimens. This particular height and width made sure that there were available scan points which would not have the edges in the scan region even at large angles of rotation. The thickness of the specimens was also key. The object was to reduce the amount of absorption and scattering with the rotations by as much as possible. However, as a flat plate like these specimens rotates, it's effective cross-sectional area increases with respect to the transducers, which means that the sound waves must traverse a longer path at higher angles. In order to minimize this effect, a width was chosen such that the distance traversed by the sound waves changed by less than the smallest possible wavelength (that is to say, the wavelength corresponding to the highest frequency generated by the scanning apparatus) at the largest angles. These specimens were kept wrapped in moist gauze while stored in a -20°C freezer.

Additionally, a 6.6 mm thick piece of aluminum was scanned in order to make a comparison between the behavior of bone and that of a truly
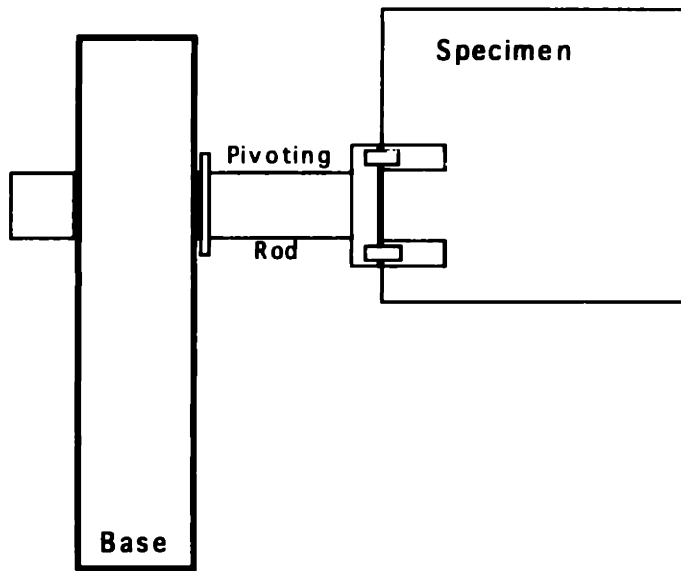
42

Figure 3-1 This is the jig for holding
the thin wafers of bone. The rod that
holds the specimen can rotate about its
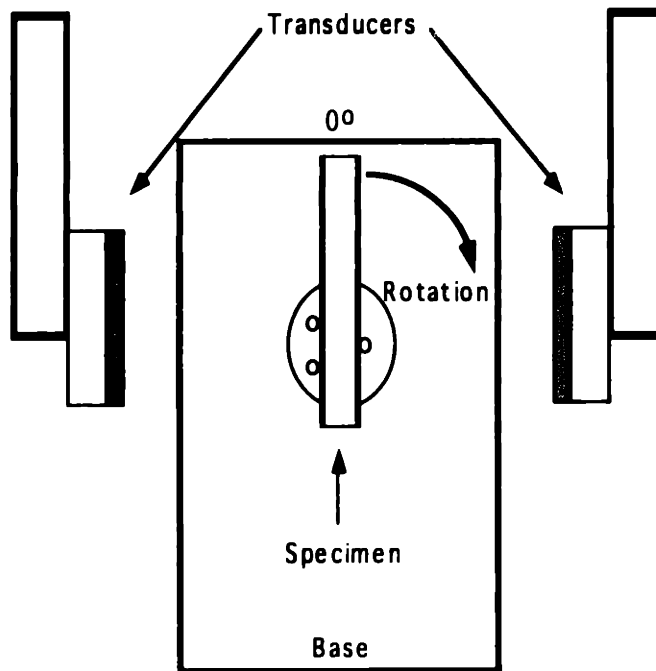longitudinal axis

Figure 3-2 Front view of jig with
respect to the transducers

homogeneous, continuous medium. Aluminum has a high characteristic impedance ($Z=17$ X 10^6 kgm^{-2}s^{-1}) and low coefficient of attenuation ($\alpha = 0.018$ dBcm^{-1} at 1 MHz). This combination plus the fact that it is a contiguous medium means that the mode of attenuation of the ultrasound waves should be almost entirely due to reflection.

3.4 Methods

The same ultrasound apparatus and water tank were used as were used described in section 1.5. However, the jig used to hold the specimens had to be different to accommodate the geometry of these specimens. The new apparatus is shown in Figures 3-1 and 3-2, it consists of a clamp mounted on a block of polyethylene that has the angle markings printed on it (angle markings created by CricketGraph). The clamp is fitted to the hole such that it is allowed to rotate, but is held firmly enough to maintain a set position. Additionally, a washer with a mark perpendicular to the clamp arm has been fitted to the clamp arm so that the rotation of the clamp can be measured. This setup allows for rotating the specimen accurately in ten degree increments with respect to the transducers.

Each specimen was degassed in a water bath for 2 hours under vacuum, after which the specimens were transferred underwater to the water bath for ultrasound scanning. The specimens were each scanned in five orientations (0°, 10°, 20°, 30°, 40°)in a similar fashion as described in the previous chapter. The attenuation of the transmitted sound waves in positions that were not affected by edge effects was recorded. In the case of where the specimens were oriented perpendicular to the path of the sound waves, the relative size of the reflected pulse to the transducer was also measured.

3.5 Results

The first type of data that was analyzed was the ultrasound attenuation at 577 kHz, and how it was affected by the rotation of the specimen. The plots
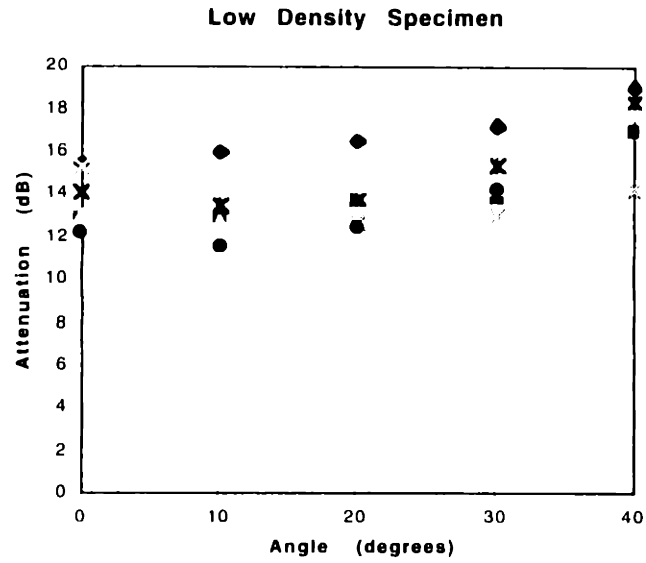
Low Density Specimen

Figure 3-3 The attenuation vs. angle plot of the low density specimens

High Density Specimen

Figure 3-4 The attenuation vs. Angle plot for the high density specimens

45

of attenuation versus angle are shown in Figures 3-3 through 3-5. These figure show that attenuation has some dependency on angle. However, qualitatively, the effect is much more pronounced in the case of the higher density specimens and the aluminum.

The reflected signals for the bone specimens and the aluminum are shown in Figures 3-6. There is a greater reflection peaks shown in the high density bone and the aluminum case than in the low density bone case.

3.6 Discussion

The result is consistent with the hypothesis that reflection is a more important factor in the high density case than in the low density case. In other words, as the wavelength of the sound wave approaches the characteristic spacing of the specimen, the attenuation is less influenced by gross reflection. Because the cross-section of the specimen is not changing by more than a wavelength in each rotation, the dependency on angle must be due to something other than the length of the cross-section (which is more important for scattering and absorption). This is particularly obvious due to the magnitude of the change in attenuation. The fact that the highly reflective aluminum piece had a qualitatively similar result as the high density bone also provides evidence for this theory.

The fact that the relative sizes of the reflected signals showed that the low density bone had a much smaller peak than the signals for the other specimens had, shows that there must be less attenuation due to reflection. However, because the absolute value of the attenuation was on the same order as that of the high density case, there is the implication that more of the attenuation in the low density bone was due to the structure of the specimen.

These results imply that gross reflection is more of a factor for the high density materials than the low density bone, which partly explains the poor performance of QUA to measure the properties of cortical bone accurately. However, it would provide more information if it were possible to use a piece
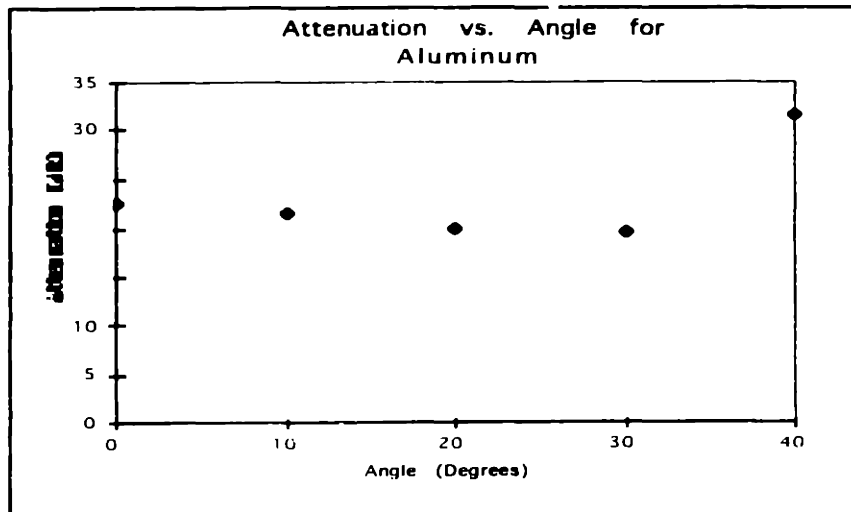
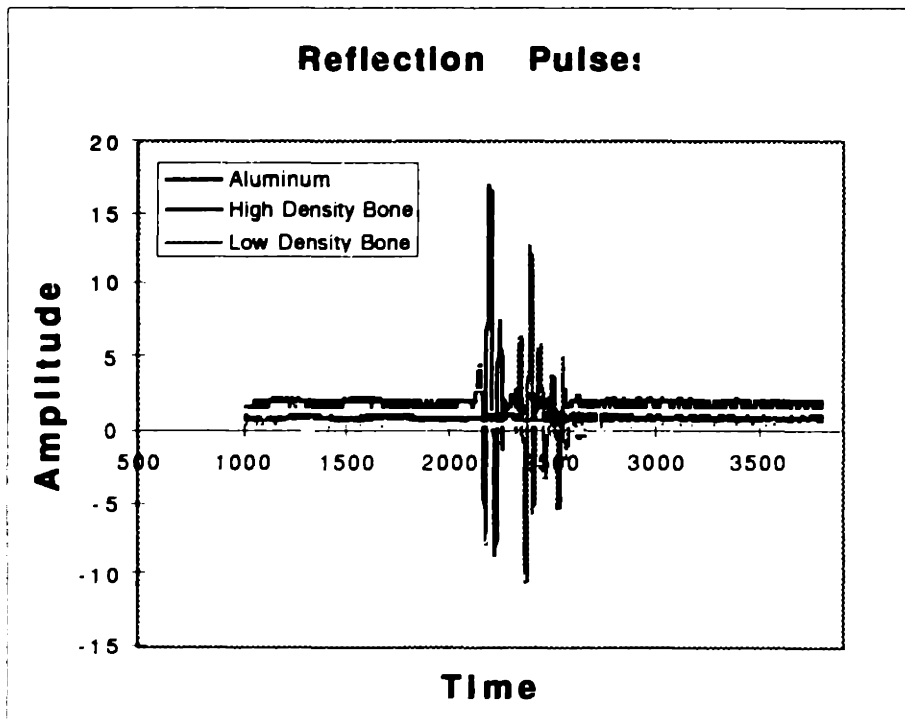Figure 3-5 Attenuation vs. Angle curve for the aluminum piece

Figure 3-6 Measured reflection pulses off of the face of the 3 types of specimen. The time axis has been shifted to emphasize peaks.

of cortical bone for this experiment to have a conclusive result.

CONCLUSIONS

The overall goal of this study was to provide evidence that it is feasible to use ultrasound attenuation to provide information as to the cross-sectional properties of bones with certain types of defects. The data suggests that it is in fact possible to use ultrasound attenuation to this end. The high correlations between measured geometric and mechanical properties with the ultrasound S1 and S2 values for the trabecular specimens is the main reason for this optimism. From these particular data, it is clear that there is information about geometric, cross-sectional properties of bone contained in the ultrasound attenuation.

The failure of the ultrasound attenuation to match these positive results for the cortical specimens indicates some of the shortcomings of the technique. However, the study described in Chapter 3 goes a long way toward explaining why the results were not as good in this case as in the trabecular case. The results do imply that it should be possible, by adjusting the frequency range, to measure the values for cortical bone.

FUTURE WORK

There are several steps that can be taken to bring this technique closer to being a viable clinical tool. The first would be to explore other frequency ranges. Specifically, a range that has the wavelength closer to the size of the haversian canals in cortical bone. Though it may not be reasonable to use the exact wavelength, at least a higher frequency must be investigated. Furthermore, using focused transducers, rather than the large, unfocused ones, may improve the resolution of the scanning by relieving the concern about volume-averaging. Next, using the relationship between velocity and modulus, it may be possible to, by using a combination of velocity information and attenuation information, calculate and analogue of rigidity from the information contained in the sound waves. Finally, one must look at more complicated cases than those studied in this work, where the specimens and defects all had simple geometries. All in all, the groundwork has been laid for continued study of this promising technique.

References

1. Silverman, "Essentials of Caffey's pediatric x-ray diagnosis," Pediatric Radiology, 1989, pg. 1216.

2. HJ Mankin, MC Gebhardt, and DS Springfield, "Orthopaedic oncology service tumor database" [Abstract], 1996.

3. J Body, "Metastatic bone disease: clinical and therapeutic aspects," Bone, Vol. 13, 1992, pp.S57-S62.

4. C Boring, T Squires, and T Tong, "Cancer statistics," Cancer J Clin, Vol. 43, 1993, pp. 7-26.

5. B Berrettoni and J Carter, "Current concepts in review: mechanisms of cancer metastasis to bone," J Bone Joint Surgery, Vol. 68A, 1986, pp. 308-312.

6. J Walls, N Bundred, and A Howell, "Hypercaclemia and bone resoprtion in malignancy," Clin Orthop, Vol 312, 1995, pp.51-63.

7. M Fidler, "Prophylactic internal fixation of secondary neoplastic deposits in long bones," British Medical J, Vol. 10, 1973, pp.341-343.

8. M Fidler, "Incidence of fracture of metastases in long bones," Acta Orthop Scand, Vol. 52, 1981, pp. 623-627.

9. K Mase, T Fukumura, J. Toriwaki, Modified Digital Voronoi Diagram and its Applications to Image Processing, Systems Computer Controls, Vol. 12, No. 6, 1981, pp 27-36.

10. R Capanna, A Dal Monte, S Gitelis, and M Campanacci, "The natural history of unicameral bone cysts after steroid injection," Clinical Orthopaedics and Related Research, 1982, pp. 204-211.

11. JJ Gartlan and FL Cole, "Modern concepts in the treatment of unicameral bone cysts of the proximal humerus," [Review], Orthopedic Clinics of North America, Vol. 6, 1975, pp.487-498.

12. PR Robins, and HA Peterson, "Management of pathologic fractures through unicameral bone cysts," JAMA, Vol. 222, 1972, pp. 80-81.

13. SJ Houston and RD Rubens, "The systematic treatment of bone metastases," Clin Orthop, Vol. 312, 1995, pp. 95-104.

14. KD Harrington, "Orthopaedic management of extremity and pelvic lesions," *Clin Orthop*, Vol. 312, 1995, pp. 76-88.

15. RB Ashman and JY Rho, "Elastic modulus of trabecular bone material," *J Biomech*, Vol. 21, pp.177-181.

16. CH Turner, M eich, "Ultrasonic velocity as a predictor of strength in bovine cancellous bone," *Calcif Tissue Int*, Vol. 49,116-119.

17. LL Wright, MJ Glade, and J Gopal, "The use of transmission ultrasonics to assess bone status in the human newborn," *Pediatric Research*, Vol. 22, 1987, pp.541-544.

18. CC Gluer, et al, "Three quantitative ultrasound parameters reflect bone structure," *Calcif Tissue Int*, Vol. 55, 1994, pp. 46-52.

19. CM Langton, SB Palmer, and RW Porter, "The measurement of ultrasonic attenuation in cancellous bone," *Engineering in Medicine*, Vol. 13, 1984, pp. 89-91.

20. EV McCloskey, SA Marray, et al, "Assessment of broadband ultrasound attenuation in the os calcis in vitro," *Clinical Science*, Vol. 78, 1990, pp. 221-225.

21. ML McKelvie, J Fordham, et al, "In vitro comparison of quantitative computed tomography and broadband ultrasonic attenuation of trabecular bone," *Bone*, Vol. 10, 1989, pp. 101-104.

22. CM Langton, SB Palmer, and RW Porter, "The measurement of broadband ultrasonic attenuation in cancellous bone," *Eng Med*, Vol. 13, 1987, pp. 89-91.

23. MB Tavakoli and JA Evans, "Dependence of the velocity and attenuation of ultrasound in bone on the mineral content," *Physics in Medicine and Biology*, Vol. 36, 1991, pp.1529-1537.

24. JA Evans and MB Tavakoli, "Ultrasonic attenuation and velocity in bone," *Physics in Medicine and Biology*, Vol. 35, 1990, pp. 1387-1396.

25. JE Barger, "Attenuation and dispersion of ultrasound in cancellous bone," in Ultrasonic Tissue Characterization II, M Linzer ed., National Bureau of Standards, Spec. Publ. 525, US Government Printing Office, Washington DC, pp. 197-201.

26. CM Langton, SB Palmer, and RW Porter, "The measurement of ultrasonic attenuation in cancellous bone," *Engineering in Medicine*, Vol. 13, 1984, pp. 89-

91.

27. Hong, JJ, "Predicting the failure load of trabecular bone with simulated osteolytic defects using magnetic resonance imaging and dual x-ray absorptiometry," Massachusetts Institute of Technology, 1997. [Master's Thesis]

28. Greenleaf, James F., <u>Tissue Characterization with Ultrasound</u> Vol. II, CRC Press, pg. 221.

29. Editors V C Mow, A Ratcliffe, and SL-Y Woo, <u>Biomechanics of Diarthrodial Joints</u>, Springer-Verlag, New York, Volume II, 1990, pp. 31-59.

30. Ashman, R. B., J. Corin, and C. Turner, "Elastic Properties of Cancellous Bone: Measurement by an Ultrasonic Technique," Vol. 20, No. 10, 1987, pp. 979-986.

31. SE Radloff, The Effects of Trabecular Architecture, Strength, and Bone Mineral Density on Calcaneal Ultrasound," [Masters Thesis], Massachusetts Institute of Technology, Cambridge, Ma., 1995.

APPENDIX A: BASICS OF ULTRASOUND

Ultrasound is a term for mechanical vibrations with frequencies (v) higher than those normally detectable by the human ear (frequencies above 20 kHz). These vibrations produce rarefactions and compressions which form a wave in a medium. A wave can be described by four parameters: velocity (c), frequency (υ), wavelength (λ), and amplitude (or energy), as shown in Figure 1. The frequencies used in clinical ultrasound typically vary between 50 kHz and 20 MHz and most bone analysis has been at frequencies lower than 5 MHz. This study looks at frequencies between 228 kHz and 577 kHz.
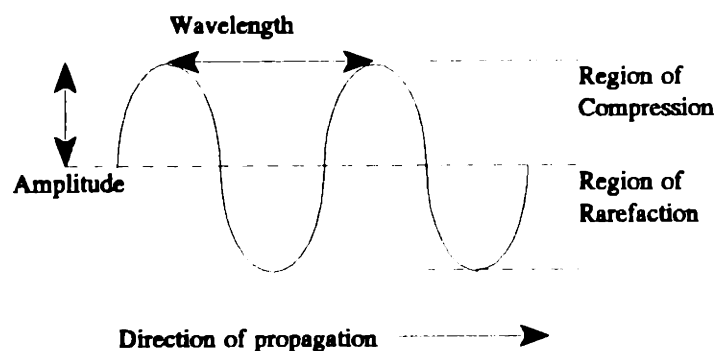

Figure 1 - Characteristics of an ultrasound wave

Ultrasound waves are generated by a transducer which is coupled to the medium through which the waves travel. There are two principle modes of propagation for sound waves. Longitudinal waves are those in which the oscillation of the particles is in the same direction as the wave's propagation. This is the most common mode by which sound travels through tissue, and it is the only mode supported by liquid media. Transverse, or shear, waves are produced when the vibration of the particles is perpendicular to the direction of the propagating wave. The transducer for this experiment produces a series

54

of elevations and depressions in the pressure due to the vibrating particles (compressions and rarefaction) which result in longitudinal waves.

There are three important acoustic parameters that are typically used to define a medium in which a sound wave propagates: speed of sound (c), characteristic impedance (Z), and attenuation coefficient (α). Speed of sound in a medium can be used to relate the wave frequency and the wavelength (λ):

$$c = \lambda v \qquad [11]$$

When the ultrasound wavelength is large compared to the characteristic lengths of the specimen and the specimen is homogeneous and non-dispersive, velocity has a direct relation to modulus:

$$c = \sqrt{\frac{E}{\rho}} \qquad [12]$$

In the case of bone, no closed-form relation like equation [2] exists. However, this equation has been used to derive first-order estimates of material properties of bone:

$$E \approx k_1 C^{2\alpha/(\alpha-1)} \qquad [13]$$

and

$$\rho \approx k_2 C^{2/(\alpha-1)} \qquad [14]$$

where k_1 and k_2 depend on E/ρ^{α} and α (the power-law relation between

modulus and density).

Characteristic impedance is related to both the density of the medium and the speed of a sound wave traveling through it:Impedance is important

$$Z = \rho c \qquad [15]$$

because it determines how much of the wave's energy is reflected at a boundary between two media. At the interface between two media of impedances Z_1 and Z_2, respectively, the amount of transmitted energy is proportional to $4Z_1Z_2/(Z_1 + Z_2)^2$ and depends on the angle of incidence of the wave with respect to the interface. According to Snell's Law, the amount of wave refraction also depends on the impedance mismatch.

The attenuation coefficient, α (dB), is the space constant in the exponential decay of the intensity of an ultrasound wave as it traverses a medium. The attenuation coefficient depends on specimen thickness; therefore the attenuation per unit thickness is expressed as the specific attenuation:

$$\mu = \alpha/d \qquad [16]$$

Ultrasound attenuation is a function of frequency, and the relationship between attenuation and frequency for bone is linear over a wide frequency range. Hence, the attenuation coefficient is often expressed by the slope of the regression line, α_1 (dB/MHz) or μ_1 (dB/cm-MHz).

Appendix B: Preliminary Studies

Quantitative ultrasonic attenuation (QUA) has been investigated not only to determine material properties of specimens, but geometric properties as well. In preparation for a protracted study of QUA, a series of initial studies were conducted to qualitatively determine the ability of ultrasound to determine geometric properties of bone specimens. These preliminary studies had four objectives:

3. Determine if the tank which houses the ultrasound apparatus confounds the ultrasonic signal in any way

4. Characterize the the raw attenuation of the ultrasound signal using a simple material in order to determine what signal is being used as an input to the Walker Sonix filtering software and whether or not the output of that software is valid and predictable.

5. Verify that the material and geometry of bone specimens do not affect the raw and filtered ultrasound signals beyond the desired attenuation.

6. Determine if the filtered signals of bone scans can qualitatively measure certain geometric and structural characteristics using QCT as the gold standard for comparison.

1.TANK STUDY

The first test determined whether or not the tank which houses the ultrasound apparatus produces any signal artifacts that could interfere with measurement of either the transmitted or reflected signal. In the test, a single ultrasonic pulse was transmitted through the water. The output of the receiving transducer was plotted versus time, showing that the transmitted signal is "clean" and that there are no spurious or delayed peaks. Therefore, it can be assumed that the ultrasound apparatus is not affected by signal artifacts

resulting from the tank architecture. The lack of a pulse in the received reflection shows that the transmission time to pulse rate ratio is fast enough for the reflected signals not to interfere with data collection.

2.TESTS ON ALUMINUM SPECIMENS

This test studied the characteristics of the ultrasound response to a simple specimen of known material and sonic properties and determined if the response was theoretically predictable. For this study, a rectangular block of aluminum (25.4 mm on a side) and a cylinder of aluminum (25.4 mm in diameter) were scanned in the following four positions in a water bath:

1. The specimen was placed equidistant from the two transducers and oriented so that its surface was normal to the transducers and, hence, to the incoming pulse.
2. The specimen was shifted so that only half of the specimen was in the scan region.
3. The specimen was positioned with its flat surfaces oriented at 45 degrees to the transducers.
4. The specimen was oriented with its surface normal to the transducers, but with the specimen located much closer to the left transducer than to the right.

Both the transmitted and reflected signals were measured and plotted versus time for each of the four specimen placements.

For the rectangular block, the first position produced a clean, easily-discerned group of peaks in both transmission and reflection. Shifting the specimen to the side increased the intensity of the signal, suggesting that the signal measured the reduction of material in its path. The received signal peaks were not smeared (spread out over a long amount of time) or offset in

time by this repositioning.

Rotating the specimen 45 degrees, however, caused the creation of many secondary peaks in the received signal. This lack of a clear peak was expected, as sound waves refract at the interface between two continua when that interface is inclined with respect to the incoming wave path. Because the transmission path of the wave was refracted, different portions of the wave passed through different amounts of the aluminum and sound travels faster in aluminum than in water, the arrival of the signal at the receiving transducer was spread out over time. The rotated orientation smeared not only the transmitted signal, but the reflected signal as well.

Shifting the specimen closer to the left transducer shortened the time to the primary reflection peak and caused a second, smaller reflection peak that occurred when part of the wave was reflected from the back face of the square aluminum specimen.

Two significant results were noted when comparing the scans of the cylindrical specimens to those of the rectangular specimens. The transmitted signal of the cylinder was significantly smeared, just as with the signal from the rectangular block oriented at 45 degrees. However, upon repositioning the specimen closer to the left transducer, a second reflected signal peak did not occur with the cylinder, unlike the response for the rectangular specimen. Both of these results suggest that there is a significant amount of refraction occurring at the inclined interface of a continuous medium.

GEOMETRIC IRREGULARITIES

This test was conducted to determine how a gross geometric irregularity affects the attenuation signal. A hole was drilled transversely through the each of the cylindrical and rectangular aluminum specimens. Two hole sizes were used: 20% and 60% of the nominal diameter of the specimen. The specimens were scanned with the long axis of the hole oriented at angles of 0, 45, 90, and 135 degrees with respect to the transducers. Both the transmitted and reflected

signals were measured, and the results were compared to those of the scans before the holes were introduced.

For the 0-degree orientation, the transmitted signals for the specimens with holes were significantly larger than the signals of specimens without holes, as indicated by the drop in gain on the plots of signal vs. time. As the hole size increased so did the transmitted signal.

However, rotating the specimen to 45, 90, and 135 degrees significantly smeared both the transmitted and reflected signals, particularly in the case of the rectangular specimen. Scans at these angles also did not produce the same increase in transmitted signal that occurred with the 0-degree scans. The first observation again suggests that significant refraction takes place at the interface of the hole and water, which is consistent with the refraction resulting from gross changes in geometry in Test 2 (such as rotating the rectangular specimen). The second observation is consistent with a significant increase in reflection associated with the sides of the defects causing the increased (compared to the 0 degree scan) attenuation.

WIDTHS

In a final study of the aluminum specimens, the post-processed signal for each of the aluminum specimens was inspected visually in AVS. The inspections yielded results similar to those discussed earlier, and further showed that a crisper image was obtained at the higher frequencies.

The width of the specimen predicted by the Walker Sonix software based on the time to receive the transmitted and reflected signals was also compared to the actual specimen width of 25.4 mm. The width was predicted at for each signal pulse and was $\mu = 24.8$ mm $\sigma = 0.244$ mm for the rectangular specimen and $\mu = 24.8$ mm $\sigma = 0.252$ mm for the cylindrical specimen. These measurements represented an error in the mean of 2.35% and 2.23%, respectively.